Applied Catalysis B: Environmental 144 (2014) 83–89

Contents lists available at ScienceDirect

Applied Catalysis B: Environmental

journal homepage: www.elsevier.com/locate/apcatb

Highly photocatalytic performance of flexible 3 dimensional (3D) ZnO nanocomposite

Hyun Uk Lee[a,*,1], So Young Park[a,1], Soon Chang Lee[b], Jung Hye Seo[a], Byoungchul Son[c], Hyeran Kim[a], Hyung Joong Yun[a], Go Woon Lee[d], Sang Moon Lee[a], Bora Nam[c], Jae Won Lee[e], Yun Suk Huh[f], Cheolho Jeon[a], Hae Jin Kim[a], Jouhahn Lee[a,**]

[a] Division of Materials Science, Korea Basic Science Institute, Daejeon 305-333, Republic of Korea
[b] New Business Development Department, SHINE Co. Ltd., Kimhae 621-823, Republic of Korea
[c] Jeonju Center, Korea Basic Science Institute, Jeonju 561-756, Republic of Korea
[d] Testing and Certification Center, Korea Institute of Energy Research, Daejeon 305-343, Republic of Korea
[e] Department of Energy Engineering, Dankook University, Cheonan 330-714, Republic of Korea
[f] Department of Biological Engineering, College of Engineering, Inha University, Incheon 402-751, Republic of Korea

ARTICLE INFO

Article history:
Received 3 March 2013
Received in revised form 8 June 2013
Accepted 21 June 2013
Available online 29 June 2013

Keywords:
Zinc oxide
Photocatalyst
Nanostructure
Photocatalytic activity

ABSTRACT

Zinc oxide (ZnO) is one of the most powerful materials for purifying organic pollutants using photocatalytic activity. In this study, we have introduced a novel method to design highly photoreactive flexible 3 dimensional (3D) ZnO nanocomposite [F-ZnO-m (m: reaction time, min)] by electrospinning and simple-step ZnO growth processing (one-step ZnO seed coating/growth processing). Significantly, the F-ZnO-m could be a new platform (or candidate) as a photocatalytic technology for both morphology control and large-area production. The highest photocatalytic degradation rate ([k]) was observed for F-ZnO-m at 2.552 h^{-1}, which was 8.1 times higher than that of ZnO nanoparticles (NPs; [k] = 0.316 h^{-1}). The enhanced photocatalytic activity of F-ZnO-m may be attributed to factors such as large surface area. The F-ZnO-m is highly recyclable and retained 98.6% of the initial decolorization rate after fifteen cycles. Interestingly, the F-ZnO-m samples show very strong antibacterial properties against both Gram-negative *Escherichia coli* (*E. coli*) and Gram-positive *Staphylococcus aureus* (*S. aureus*) after exposure to UV-light for 30 min. The antibacterial properties of F-ZnO-m samples are more effective than those of ZnO NPs. More than 96.6% of the *E. coli* is sterilized after ten cycles. These results indicate that F-ZnO-m samples might have utility in several promising applications such as highly efficient water/air treatment and inactivation of pathogenic microorganisms.

© 2013 Elsevier B.V. All rights reserved.

1. Introduction

Because environmental pollution has exceeded the capacity of natural remediation processes, semiconductor-based photocatalytic reactions draws intense interests as the replacing methods for air and water purification [1–3]. Zinc oxide (ZnO), with a direct wide bandgap (DE = 3.37 eV), is highly important for the photocatalytic generation of hydrogen peroxide, useful for degrading organic pollutants [4,5], and removing bacterial contamination [6–10]. Since the reaction occurs at the interface of the photocatalyst surface and organic pollutant, the crystal morphology and structure of ZnO may have a significant effect on its photocatalytic activity [3,6,10,11]. However, the use of ZnO for the photocatalytic degradation of toxic chemicals, including chemical warfare agents, faces many challenges including maximizing the reaction efficiency in natural sunlight or UV radiation, achieving immobilization on appropriate substrates, and ensuring sufficient activity while preventing the degradation of the substrate [3,11,12]. To enhance the photocatalytic activity of ZnO, a large surface area and highly crystalline structure are required by physicochemical engineering at atomic level. In order to fulfill those requirements, manipulation of ZnO such as either decreasing the particle size and increasing the surface to volume ratio have been employed by number of research groups [1–5].

Electrospinning is a popular method to fabricate continuous ultrafine fibers with nanometer and submicrometer diameters from polymer solutions or melts [13,14]. Previously, ZnO nanofibers

* Corresponding author. Tel.: +82 42 865 3637; fax: +82 42 865 3610.
** Corresponding author. Tel.: +82 42 865 3613; fax: +82 42 865 3610.
E-mail addresses: leeho@kbsi.re.kr, biolhu@hanmail.net (H.U. Lee), jouhahn@kbsi.re.kr (J. Lee).
[1] Both these authors contributed equally.

0926-3373/$ – see front matter © 2013 Elsevier B.V. All rights reserved.
http://dx.doi.org/10.1016/j.apcatb.2013.06.030

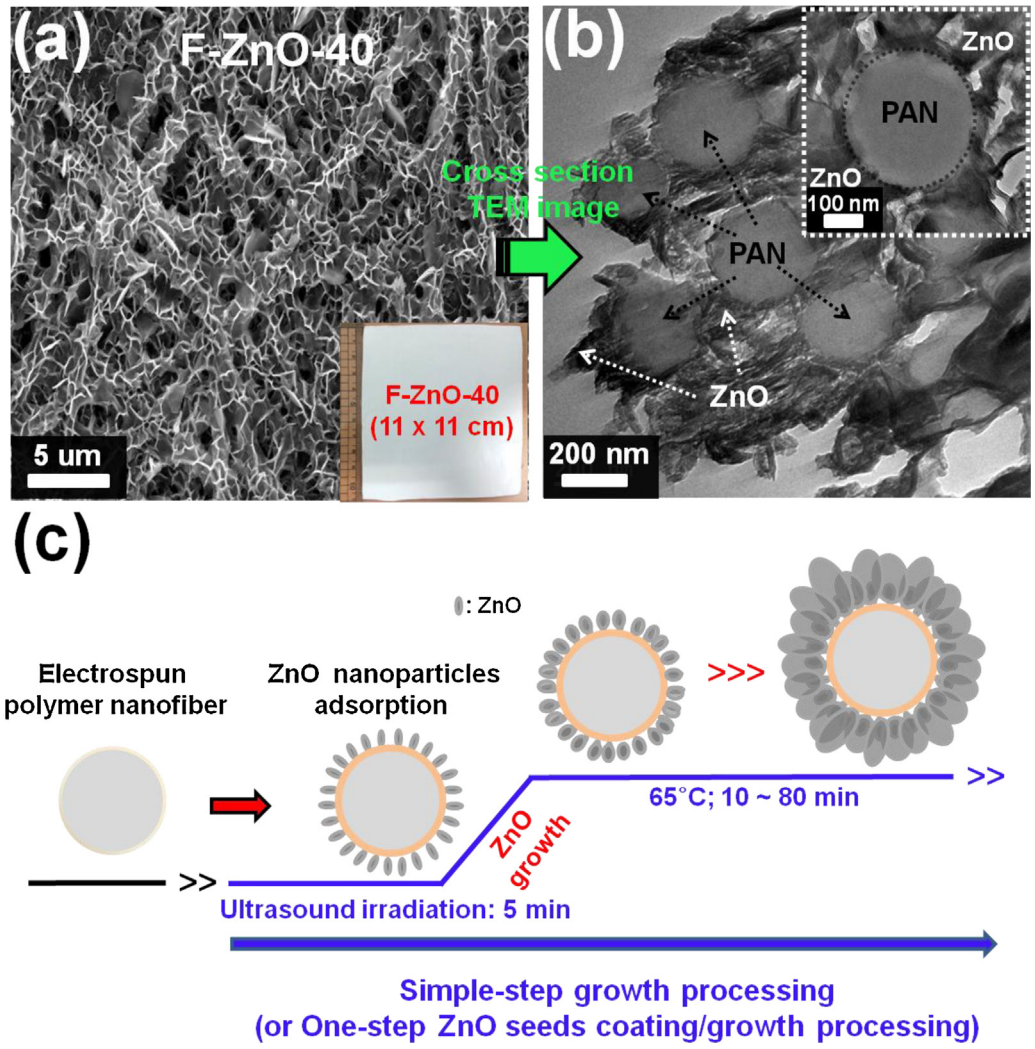

Fig. 1. (a) FE-SEM and (b) cross-section HR-TEM images of F-ZnO-40, and (c) schematic illustrating F-ZnO-m (m: reaction time, min) preparation using simple-step growth processing. The inset shows images of the F-ZnO-40 sample (size: 11 cm × 11 cm).

(NFs) have been produced by electrospinning the mixtures of polymers and ZnO precursors, such as poly(vinylpyrrolidone) with zinc acetate. However, ZnO NFs prepared by electrospinning are quite brittle owing to their polycrystalline nature are apparently unsuitable for photocatalytic applications until after calcination [14], which forms polycrystalline ZnO NFs. Therefore, there are few reports of depositing well-characterized ZnO nanoparticles (NPs) directly onto submicrometer-diameter fibers at room temperature as post-treatment [13,14]. Furthermore, ZnO nanowire arrays and nanorods were recently grown on flat polymer substrates (films) or inorganic NFs by a simple seeding method [15–18].

Herein, we first report on a novel method to prepare a highly photoreactive flexible 3 dimensional (3D) ZnO nanocomposite [F-ZnO-m (m: reaction time, min)] which retains potential applications as a photocatalyst, sensing material, electrode, or antibacterial/antiviral agent. F-ZnO-m was fabricated at low temperature (65 °C) with controlled seed adsorption by using electrospinning and simple-step growth processing (or one-step ZnO seed coating/growth processing). The F-ZnO-m exhibited very high photocatalytic activity toward the oxidation of azo dyes [i.e., reactive black 5 (RB 5) and rhodamine B (Rho B)] and efficient sterilization (or killing) of bacteria [i.e., Gram-negative *Escherichia coli* (*E. coli*) and Gram-positive *Staphylococcus aureus* (*S. aureus*)].

2. Experimental

2.1. Fabrication of F-ZnO-m

All reagents were analytical grade (Sigma–Aldrich Co., USA) and used without further purification. A 16.5 wt% polyacrylonitrile (PAN) solution was prepared by dissolving PAN in N,N-dimethylformamide (DMF) and stirring the solution for 24 h at room temperature. This solution was used to fabricate NFs by electrospinning. A voltage of 14.5 kV was applied between the needle tip and the sample plate (size: 11 cm × 11 cm) on the aluminum collector. A pump with a 5 ml syringe was used for electrospinning the PAN solution; the needle diameter was 0.15 mm and the feed rate was 0.8 ml/h. Subsequently, the solution was directly electrospun on the sample plate. In this study, $ZnAc_2$ and hexamethylenetetramine (HMT, Junsei, Japan) were used as precursors for Zn^{2+} and OH^- ions, respectively. To produce ZnO nanoleaves (NLs) during the initial reaction, mixtures of 10 mM ZnAc and 10 mM aqueous HMT

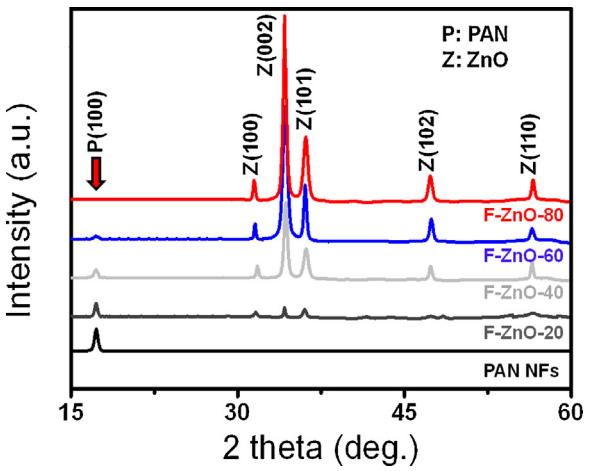

Fig. 2. XRD patterns of PAN NFs and F-ZnO-m (m: reaction time, min).

solution were prepared at room temperature. These solutions were stirred for 10 min, after which PAN NFs were added. The solution was treated for 5 min with ultrasound at 40 kHz (Ultrasonics UC-05, Lab Companion, Korea). The solution was maintained at 65 °C for 80 min to grow ZnO NLs on PAN NFs. After reaction completion, the F-ZnO-m samples were removed from the solution, rinsed with deionized water, and dried in high purity Ar gas.

2.2. Characterization

The crystalline structures of the PAN NFs and F-ZnO-m samples were investigated by X-ray diffraction (XRD; Rigaku RDA-γA X-ray diffractometer, Japan) using Cu Kα radiation with a nickel filter. The morphologies of the F-ZnO-m samples were evaluated by field emission-scanning electron microscope (FE-SEM; Hitachi S-4700, Japan) and high resolution-transmission electron microscopy (HR-TEM; JEOL JEM 2200, Japan). The Brunauer–Emmett–Teller (BET) surface areas of the F-ZnO-m samples were determined using a BET analyzer (Micromeritics ASAP 2020, Norcross, GA, USA). High resolution-X-ray photoelectron spectroscopy (HR-XPS) with

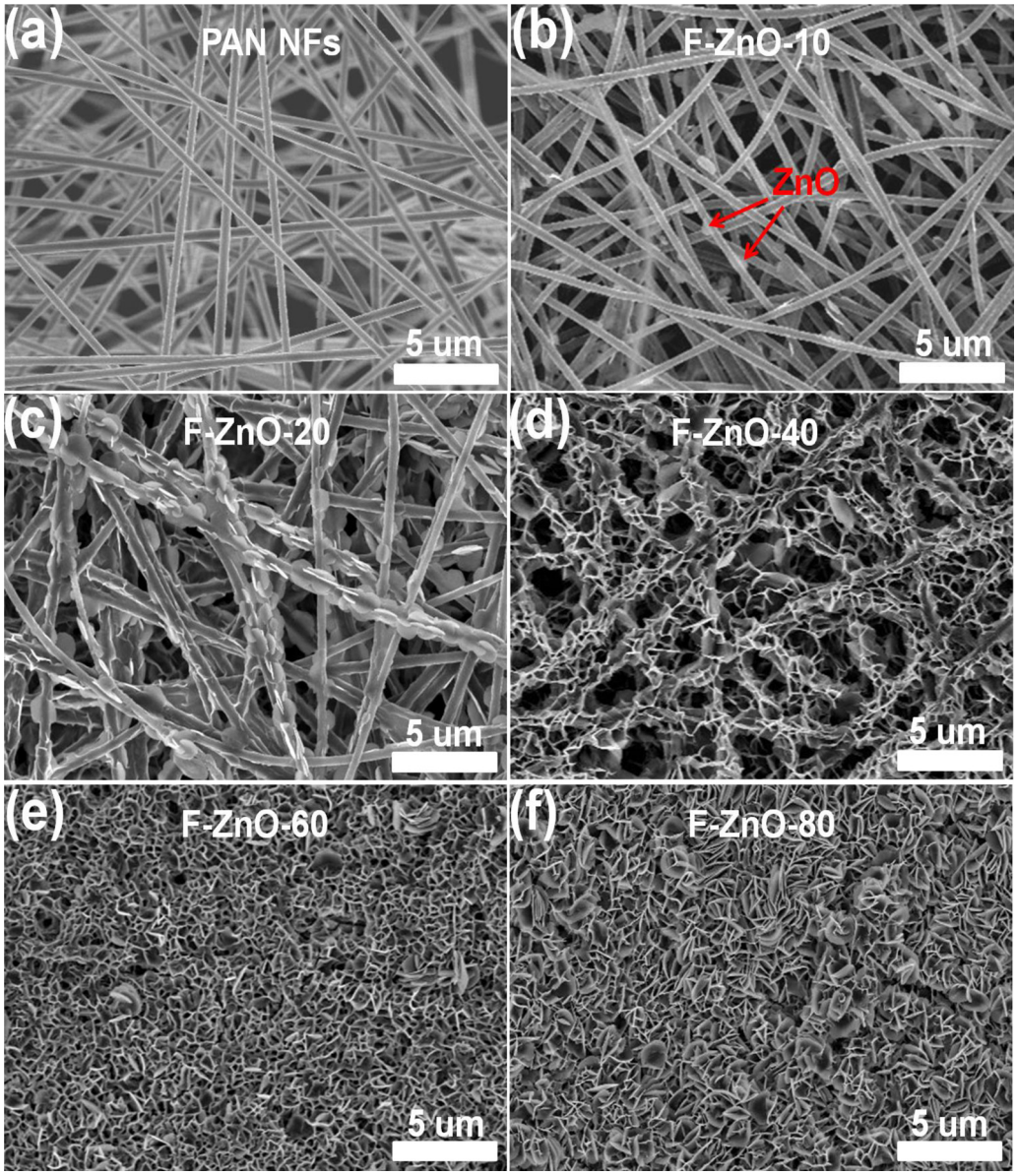

Fig. 3. FE-SEM images of (a) PAN NFs and (b–f) F-ZnO-m (m: reaction time, min).

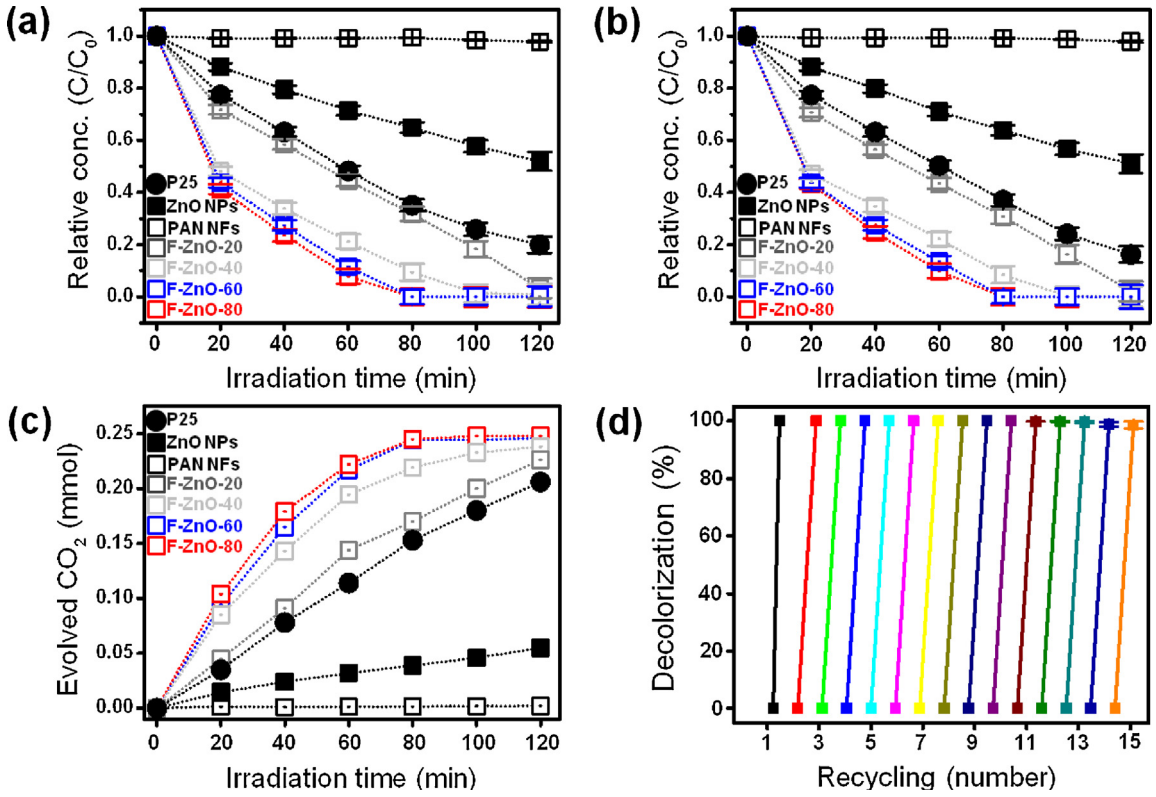

Fig. 4. Comparison of the photocatalytic behavior of P25, ZnO NPs, PAN NFs, and F-ZnO-m (m: reaction time, min) in the decomposition of (a) RB 5 and (b) Rho B solutions under UV irradiation, (c) evolution of CO_2 from RB 5 as a function of UV irradiation time (min) by photocatalytic reaction with samples, and (d) recycling results for the F-ZnO-80 sample in the decolorization of RB 5 solution.

monochromatic Al Kα X-ray radiation ($h\nu$ = 1486.6 eV) operated at 120 W (Kratos Analytical, AXIS Nova, Manchester, UK) was used to investigate the surface properties of the samples. The shift of the binding energy due to relative surface charging was corrected using the C 1s level at 284.6 eV as an internal standard.

2.3. Measurement of photocatalytic and antibacterial activities

The photocatalytic degradation of RB 5 (3 mg L^{-1}, pH 6.67, Aldrich) and Rho B (3 mg L^{-1}, pH 5.5, Aldrich) by the catalysts [0.5 g L^{-1}; P25, ZnO NPs (~25 nm, 99.8%, RND Korea Co.), PAN, F-ZnO-20, F-ZnO-40, F-ZnO-60 and F-ZnO-80], were carried out under UV irradiation (source: 4 W, 365 nm, VSLAB VL-4CL, Korea), and the absorbance of the solutions was measured using a UV-Vis-NIR spectrophotometer (Varian, Cary 5000, Australia) in the range 200–800 nm [19,20]. The concentrations of RB 5 and Rho B in the solutions after photoirradiation were measured from the peak absorbances of the solutions at 598 and 555 nm, respectively. Evolved CO_2 was analyzed with a TM IGC120-MB gas chromatograph equipped with a Q column. The recycling tests were performed after washing the recovered F-ZnO-80 twice with distilled water.

The antibacterial activity of the catalysts was evaluated by the inhibition of *E. coli* and *S. aureus* under UV irradiation [19,21–23]. Before these tests, glassware was sterilized by autoclaving at 120 °C for 15 min. Bacterial cultures were grown overnight in LB media at 37 °C with continuous shaking at ~200 rpm. The antimicrobial effects of the F-ZnO-m samples were determined by two methods: (i) antibacterial test in liquid medium, and (ii) zone of inhibition test. For the antibacterial tests in liquid medium, sterilized LB medium (5 mL) was measured into sterile tubes. The mass of the F-ZnO-m samples was adjusted to 10 mg. The treated bacterial cells were diluted to a cell suspension of ~1×10^5 colony-forming units (CFU, mL^{-1}) with deionized water. The mixtures were cultured overnight at 37 °C in a shaking incubator at 250 rpm. For the zone of inhibition tests, nutrient agar was poured onto disposable sterilized Petri dishes and allowed to solidify; 100 μl of *E. coli* bacterial suspension was streaked over the plate and was uniformly spread. F-ZnO-m samples with 5 mg weight were gently placed over the solidified agar gel at different locations on the same Petri dish. Plates were incubated at 37 °C for 12 h.

For the photocatalytic activity and antibacterial tests, the data were averaged and expressed as mean ± standard deviation. Each test was repeated up to five times. A statistical analysis was performed using analysis of variance (ANOVA), with $p < 0.05$ considered to be significant.

3. Results and discussion

3.1. Structural and physicochemical properties of F-ZnO-m samples

As shown in Fig. 1, the one-dimensional ZnO nanostructures (NSs) were fabricated directly onto electrospun polymer (polyacrylonitrile; PAN) NFs in the form of a three-dimensional structure using simple-step growth processing. The ZnO NLs can be continuously grown on PAN NFs (F-ZnO-m) via the immobilization of ZnO seeds onto PAN NFs by simple-step growth processing with ultrasound irradiation. By combining the properties of one- and three-dimensional NSs, F-ZnO-m may emerge as a more interesting material than simple arrays of NLs because of their higher specific surface area, flexibility, and porosity, especially for applications in

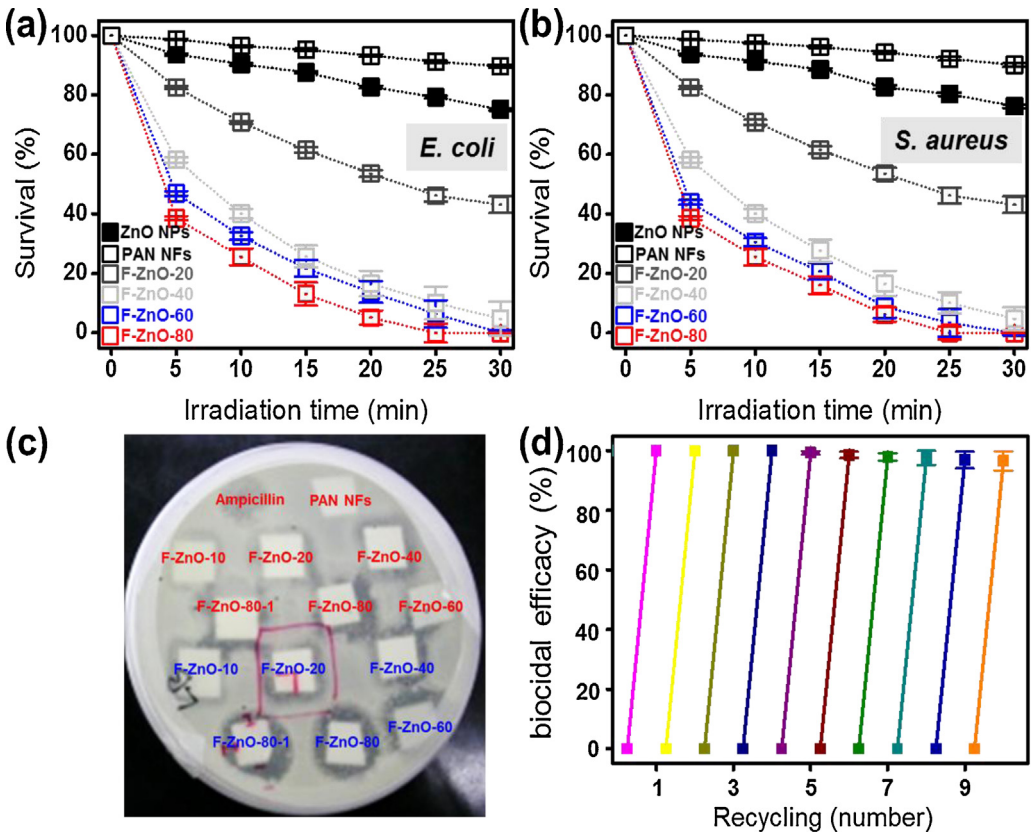

Fig. 5. Plot of survival (%) versus UV irradiation time (min) for ZnO NPs, PAN NFs, and F-ZnO-m (m: reaction time, min) against (a) *E. coli* and (b) *S. aureus*; and (c) bacterial inhibition results and (d) biocidal efficacy of the F-ZnO-80 sample against *E. coli*.

sensing, photocatalysis, and semiconductor-sensitized solar light harvesting.

Fig. 2 shows XRD patterns of the ZnO NLs grown on PAN NFs as a function of reaction time (0–80 min). For pure PAN NFs, the main peak associated with the (1 0 0) plane of NFs appeared at 2θ values of ~17°. The main peak intensity decreased as the reaction progressed, indicating the disruption of NFs' orientation and crystalline structure by the growth of ZnO NLs [24–26]. The peak intensities of ZnO in the XRD pattern increased with the increasing reaction time for the formation of ZnO NLs. Because of the NLs on the PAN NFs were considered to be (0 0 2)-oriented ZnO crystals with different growth directions due to the rough surface of the PAN NFs. The diffraction peaks were indexed to a wurtzite ZnO structure with lattice constants $a = 0.3249$ nm and $c = 0.5206$ nm (JCPDS card: 36–1451) [13,27,28].

Fig. 3 shows the FE-SEM images and growth behavior of the ZnO NSs grown on PAN NFs as a function of the reaction time (0–80 min). All the ZnO NSs had NLs morphology, regardless of the growth time (Fig. 3b–f). The ZnO NLs within a local region seem to be randomly oriented, while the NPs are aligned preferentially parallel to the *c*-axis along the leaf. The growth behavior of F-ZnO-m can be explained as follows. First, ZnO NPs are nucleated on the PAN NF surface during the primary 5 min of ultrasound irradiation. The surface of the ultrasound-irradiated PAN NFs is negatively charged owing to ionized hydroxyl groups (see Figs. S1 and S2 in Supporting Information). Coulombic forces then locally bind the Zn^{2+} ions to the PAN NF surfaces. Then, $Zn(OH)_2$ is continuously produced on the surface by incorporating OH^- ions from the solution (see Fig. S1 in Supporting Information). Decomposition of $Zn(OH)_2$ following the reaction $Zn(OH)_2 \rightarrow ZnO + H_2O$, produce ZnO under ultrasound irradiation (see Table S1 in Supporting Information). The ZnO seeded PAN NF offer low energy nucleation sites enabling easy heterogeneous formation of ZnO nuclei over it, and growth of these nuclei taking $Zn(OH)_2$ complexes as the precursor occur at the later stage. The wurtzite ZnO structure may be viewed as composed of stacked alternate planes composed of Zn^{2+} and O^{2-} ions and this peculiar stacking leads to different surface energy of the crystal planes which resulted in the main growth direction of the ZnO is in [0 0 1] direction. [29–31]. The (0 0 2) plane of ZnO, a polar crystal, is rich in Zn and O atoms whose surface dipoles are thermodynamically unstable, yielding a higher crystal growth rate to reduce their surface energy [29–31]. During the simple-step growth processing, strong electrostatic attraction promotes the adsorption of the growth unit of ZnO onto the polar (0 0 2) plane, resulting in faster growth along the [0 0 1] direction [13,31].

3.2. Photocatalytic and antibacterial activities of F-ZnO-m samples

To confirm the photocatalytic performance of the P25, ZnO NPs, PAN NFs, and F-ZnO-m, the decolorization of RB 5 and Rho B solutions diluted in water was investigated under UV irradiation (Fig. 4). In the case of F-ZnO-60 and F-ZnO-80, the RB 5 and Rho B solutions degraded almost entirely and became transparent within 80 min (Fig. 4a and b). The solutions containing P25, ZnO NPs, PAN, F-ZnO-10, and F-ZnO-20 were still somewhat blue (RB 5) or red (Rho B) after 120 min. No change was observed in the absorbance of dye solutions irradiated without photocatalysts. The highest photocatalytic degradation rate ([*k*]) was observed for F-ZnO-80 at 2.552 h^{-1}, which was 8.1 times higher than that of ZnO

NPs ($[k] = 0.316\ h^{-1}$) (see Table S2 in Supporting Information). The enhanced photocatalytic activity of three-dimensional ZnO may be attributed to factors such as large surface area [1,3,32–34]. The large surface area of F-ZnO-80 generally induces higher photocatalytic activity by better adsorptive capacity for azo-dye particles (see Table S3 in Supporting Information) and providing more hydroxyl radicals in photocatalytic reaction [1,3,35]. By irradiating of UV light on F-ZnO-m, conduction-band electrons and valence-band holes were generated on the surfaces of ZnO NLs. The hydroxyl radicals were formed with the reaction between valence-band holes and water molecules adhering to the surfaces of ZnO NLs [35–37]. The excited electrons also react with oxygen molecules to form superoxide radicals, which subsequently react with protons to produce hydroxyl radicals [36,37]. Hydroxyl radicals are active oxidizers capable of degrading organic pollutants. At the beginning of degradation process, reaction rate was faster for the number of hydroxyl radicals increased gradually [35,37].

Fig. 4c shows the increase in evolved CO_2 with time during the photocatalytic reaction of RB 5 with the P25, ZnO NPs, PAN NFs, and F-ZnO-m samples under UV irradiation. After UV irradiation for 120 min, the samples with F-ZnO-80 had evolved 6.2 times more CO_2 than those with ZnO NPs (0.243 mmol versus 0.039 mmol CO_2), indicating that a high degree of mineralization for RB 5 was achieved. The length of one cycle was 0–120 min (UV irradiation time), and decolorization was measured at every time (Fig. 4d). After fifteen cycles of the degradation reaction, the photocatalytic conversion ratio of RB 5 for the F-ZnO-80 retained approximately 98.6% under UV irradiation. F-ZnO-80 clearly exhibits excellent photocatalytic stability, yielding efficient removal of organic contaminants even after 15 cycles. No significant change also was observed in the XRD patterns of F-ZnO-80 before and after photocatalytic reaction (Fig. S3).

Fig. 5 shows the antibacterial activities of the PAN NFs, ZnO NPs, and F-ZnO-m samples against Gram-negative *E. coli* and Gram-positive *S. aureus* under UV irradiation. The dark controls (F-ZnO-m samples + bacteria in dark) showed that F-ZnO-m samples have no microbicidal activity under dark conditions. Bacterial survival was calculated by percentage survival ($=B/A \times 100$; A, number of surviving microbial colonies in the absence of irradiation; B, number of surviving colonies in the presence of UV irradiation). After 5 min of irradiation, ZnO NPs exhibited ~93.7% survival of *E. coli*, whereas F-ZnO-80 was nearly tenfold as active, exhibiting 38.6% survival (Fig. 5a). This may be due to the higher concentration of OH radicals, which are very strong oxidative species against microbes on F-ZnO-m samples [18,38,39]. Fig. 5a shows that *E. coli* can be almost completely killed within 25 min on F-ZnO-80 under UV irradiation. For ZnO NPs, ~75.2% bacterial survival of *E. coli* bacteria was observed after 30 min of irradiation owing to the relatively lower surface area of the NPs. A similar result was observed in the antibacterial test against *S. aureus* (Fig. 5b). The bacterial inhibition results showed that the F-ZnO-m samples exhibited higher antibacterial activity compared to PAN NFs when exposed to UV irradiation (Fig. 5c). Moreover, the recycle runs indicate good stability of F-ZnO-80 (Fig. 5d). After 10 consecutive tests, the kill percentages of the bacteria were still as high as 96.6% for *E. coli*. From these results, it was concluded that relative to the metal oxide NSs/polymer NSs, the F-ZnO-m samples had excellent antibacterial properties against both Gram-negative and Gram-positive bacteria owing to their synergic bactericidal performance.

4. Conclusions

In conclusion, we have demonstrated the facile preparation of photocatalytically active F-ZnO-m with large surface area by using simple-step growth process (or one-step ZnO seeds coating/growth processing) at low temperature (65 °C). The photocatalytic activities of F-ZnO-m samples were found to be significantly higher than those of ZnO NPs and PAN NFs. The recycling of photocatalytic activity of the F-ZnO-m sample used in this study was excellent. Moreover, F-ZnO-m exhibited remarkable antibactericidal activity toward Gram-negative *E. coli* and Gram-positive *S. aureus*. These results suggest promising applications for F-ZnO-m in water treatment, inactivation of pathogenic microorganisms, protective clothing systems, contaminant separations, and self-antifouling systems.

Acknowledgments

This research was supported by the Converging Research Center Program through the Ministry of Education, Science and Technology (2012K001302).

Appendix A. Supplementary data

Supplementary data associated with this article can be found, in the online version, at http://dx.doi.org/10.1016/j.apcatb.2013.06.030.

References

[1] A. Kubacka, M. Fernández-García, G. Colón, Chemical Reviews 112 (2012) 1555–1614.
[2] H. Chen, C.E. Nanayakkara, V.H. Grassian, Chemical Reviews 112 (2012) 5919–5948.
[3] H. Tong, S. Ouyang, Y. Bi, N. Umezawa, M. Oshikiri, J. Ye, Advanced Materials 24 (2012) 229–251.
[4] X. Wang, M. Liao, Y. Zhong, J.Y. Zheng, W. Tian, T. Zhai, C. Zhi, Y. Ma, J. Yao, Y. Bando, D. Golberg, Advanced Materials 24 (2012) 3421–3425.
[5] A. Mclaren, T. Valdes-Solis, G. Li, S.C. Tsang, Journal of American Chemical Society 131 (2009) 12540–12541.
[6] J. Lee, S. Mahendra, P.J.J. Alvarez, ACS Nano 4 (2010) 3580–3590.
[7] J.T. Seil, T.J. Webster, Nanotechnology 23 (2012), 495101(1–9).
[8] K.R. Raghupathi, R.T. Koodali, A.C. Manna, Langmuir 27 (2011) 4020–4028.
[9] V.B. Schwartz, F. Thétiot, S. Ritz, S. Pütz, L. Choritz, A. Lappas, R. Förch, K. Landfester, U. Jonas, Advanced Functional Materials 22 (2012) 2376–2386.
[10] G. Applerot, A. Lipovsky, R. Dror, N. Perkas, Y. Nitzan, R. Lubart, A. Gedanken, Advanced Functional Materials 19 (2009) 842–852.
[11] S. Meng, D. Li, X. Zheng, J. Wang, J. Chen, J. Fang, Y. Shao, X. Fu, Journal of Materials Chemistry A General 1 (2013) 2744–2747.
[12] D.S. Bohle, C.J. Spina, Journal of American Chemical Society 131 (2009) 4397–4404.
[13] H.U. Lee, K. Ahn, S.J. Lee, J.P. Kim, H.G. Kim, S.Y. Jeong, C.R. Cho, Applied Physics Letters 98 (2011), 193114 (1–3).
[14] M. Ahmad, J. Zhu, Journal of Materials Chemistry 21 (2011) 599–614.
[15] Z.H. Li, Y.X. Luan, Q.Z. Wang, G.S. Zhuang, Y.X. Qi, Y. Wang, C.G. Wang, Chemical Communications 41 (2009) 6273–6275.
[16] Y.H. Li, J. Gong, Y.L. Deng, Sensors and Actuators A 158 (2010) 176–182.
[17] L. Baeten, B. Conings, J. D'Haen, A. Hardy, J.V. Manca, M.K.V. Bael, Solar Energy Materials and Solar Cells 107 (2012) 230–235.
[18] P. Ravirajan, A.M. Peiró, M.K. Nazeeruddin, M. Graetzel, D.D.C. Bradley, J.R. Durrant, J. Nelson, Journal of Physical Chemistry B 110 (2006) 7635–7639.
[19] H.U. Lee, S.C. Lee, S.H. Choi, B. Son, S.J. Lee, H.J. Kim, J. Lee, Applied Catalysis B: Environmental 129 (2013) 106–113.
[20] H.U. Lee, K. Ahn, S.Y. Jeong, C.R. Cho, J.P. Kim, J.S. Bae, H.G. Kim, S.H. Kwon, H.W. Lee, Applied Physics Letters 97 (2010), 223111 (1–3).
[21] H. Kong, J. Song, J. Jang, Environmental Science and Technology 44 (2010) 5672–5676.
[22] J. Ren, W. Wang, S. Sun, L. Zhang, L. Wang, J. Chang, Industrial Engineering and Chemical Research 50 (2011) 10366–10369.
[23] D.B. Hamal, J.A. Haggstrom, G.L. Marchin, M.A. Ikenberry, K. Hohn, K.J. Klabunde, Langmuir 26 (2010) 2805–2810.
[24] D. He, C. Wang, Y. Bai, B. Zhu, Journal of Materials Science and Technology 21 (2005) 376–380.
[25] S. Lee, J. Kim, B.C. Ku, J. Kim, H.I. Joh, Advanced Chemical Engineering Science 2 (2012) 275–282.
[26] L. Tan, H. Chen, D. Pan, N. Pan, European Polymer Journal 45 (2009) 1617–1624.
[27] B.Q. Cao, T. Matsumoto, M. Matsumoto, M. Higashihata, D. Nakamura, T. Okada, Journal of Physical Chemistry C 113 (2009) 10975–10980.
[28] C. Ye, Y. Bando, G. Shen, D. Golberg, Journal of Physical Chemistry B 110 (2006) 15146–15151.

[29] Z. Zhang, H. Sun, X. Shao, D. Li, H. Yu, M. Han, Advanced Materials 17 (2005) 42–47.
[30] K. Govender, D.S. Boyle, P.B. Kenway, P.B. O'Breien, Journal of Materials Chemistry 14 (2004) 2575–2591.
[31] Y. Masuda, K. Kato, Crystal Growth and Design 9 (2009) 3083–3088.
[32] H. Sun, Y. Yu, J. Luo, M. Ahmad, J. Zhu, CrystEngComm 14 (2012) 8626–8632.
[33] K. Lee, D. Kim, P. Roy, I. Paramasivam, B.I. Birajdar, E. Spiecker, P. Schmuki, Journal of American Chemical Society 132 (2010) 1478–1479.
[34] D.S. Kim, S.Y. Kwak, Applied Catalysis A: General 323 (2007) 110–118.
[35] M.R. Hoffmann, S.T. Martin, W. Choi, D.W. Bahnemann, Chemical Reviews 95 (1995) 69–96.
[36] N. Kislov, J. Lahiri, H. Verma, D.Y. Goswami, E. Stefanakos, M. Batzill, Langmuir 25 (2009) 3310–3315.
[37] R. Qiu, D. Zhang, Y. Mo, L. Song, E. Brewer, X. Huang, Y. Xiong, Journal of Hazardous Materials 156 (2008) 80–85.
[38] J.C. Yu, W.K. Ho, J.G. Yu, H. Yip, P.K. Wong, J.C. Zhao, Environmental Science and Technology 39 (2005) 1175–1179.
[39] T.M. Tsai, H.H. Chang, K.C. Chang, Y.L. Liu, C.C. Tseng, Journal of Chemical Technology and Biotechnology 85 (2010) 1642–1653.